MOLECULAR AND CELLULAR BIOLOGY, July 2005, p. 5904–5919 Vol. 25, No. 14
0270-7306/05/$08.00+0 doi:10.1128/MCB.25.14.5904–5919.2005

Double-Strand Break Formation by the RAG Complex at the Bcl-2 Major Breakpoint Region and at Other Non-B DNA Structures In Vitro†

Sathees C. Raghavan,[1,2,3,4,5] Patrick C. Swanson,[6] Yunmei Ma,[1,2,3,4,5] and Michael R. Lieber[1,2,3,4,5]*

Norris Comprehensive Cancer Center[1] and Departments of Pathology,[2] Biochemistry & Molecular Biology,[3] Biological Sciences,[4] and Molecular Microbiology & Immunology,[5] University of Southern California Keck School of Medicine, 1441 Eastlake Ave., Los Angeles, California 90033, and Department of Medical Microbiology and Immunology, Creighton University Medical Center, 2500 California Plaza, Omaha, Nebraska 68178[6]

Received 22 November 2004/Returned for modification 30 December 2004/Accepted 10 April 2005

The most common chromosomal translocation in cancer, t(14;18) at the 150-bp bcl-2 major breakpoint region (Mbr), occurs in follicular lymphomas. The bcl-2 Mbr assumes a non-B DNA conformation, thus explaining its distinctive fragility. This non-B DNA structure is a target of the RAG complex in vivo, but not because of its primary sequence. Here we report that the RAG complex generates at least two independent nicks that lead to double-strand breaks in vitro, and this requires the non-B DNA structure at the bcl-2 Mbr. A 3-bp mutation is capable of abolishing the non-B structure formation and the double-strand breaks. The observations on the bcl-2 Mbr reflect more general properties of the RAG complex, which can bind and nick at duplex–single-strand transitions of other non-B DNA structures, resulting in double-strand breaks in vitro. Hence, the present study reveals novel insight into a third mechanism of action of RAGs on DNA, besides the standard heptamer/nonamer-mediated cleavage in V(D)J recombination and the in vitro transposase activity.

The causes of spontaneous chromosomal translocations in the somatic cells of biological organisms are largely unknown, though double-strand DNA breaks (DSBs) are required in all proposed mechanisms (18, 20). How the DNA breaks are generated has been unclear. V(D)J recombination between inappropriate sites is one defined cause of translocations, which is specific to lymphoid cells (15). Mistakes during class switch recombination are less well understood, as the physiologic target for this process is only now being elucidated (36, 43). Other mechanisms are mostly conjectural or based on circumstantial evidence. For example, when topoisomerase inhibitors are used as chemotherapeutic agents, secondary leukemias may arise that contain translocations (7). These translocations are speculated, quite plausibly, to be due to incomplete topoisomerase reactions at the breakpoints. A more general mechanism of DSB formation is replication across an unrepaired nick. Possible causes of nicks in DNA are numerous. Nicks and DSBs may arise from free radicals secondary to oxidative metabolism (8, 14). Yet another mechanism of translocations that was described recently is breakage-induced replication (26). All mechanisms proposed must account for how two breaks occur in different parts of the genome and become intermixed, and this is unclear in essentially all cases except for those mediated by V(D)J recombination. Some mechanisms, such as breakage-induced replication, can only account for nonreciprocal translocations (26), yet many translocations are reciprocal.

Immunoglobulin diversity is generated by a process called V(D)J recombination. The RAG complex, containing RAG1 and RAG2, is the enzymatic complex responsible for the DNA cleavage phase of V(D)J recombination. This process is directed by the recombination signal sequences. Recombination signals consist of conserved heptamer and nonamer sequences separated by less-conserved spacer sequences of either 12 or 23 bp. Based on the length of spacer sequences, recombination signal sequences can be classified as 12- or 23-signals. During the process of V(D)J recombination, the RAG complex brings two signal sequences together (synapsis) and cleaves them at the 5′ end of the heptamer at its junction with the V, D, or J coding end (9, 10).

We and others have shown that some of the lymphoid translocations and deletions, such as LMO2, Ttg-1, SIL, and SCL (TAL1), appear to be due to misrecognition of signal-like sequences by RAG complexes (19, 23, 29). These studies confirmed the previous suspicion that some breakpoint sites can be misrecognized as heptamer/nonamer signals. However, many of the common translocation sites are exceptions to this mechanism and do not seem to be due to heptamer/nonamer misrecognition. Examples include the bcl-2 translocation, the bcl-1 translocation, the bcr/abl translocation, and the c-*myc* translocation (30).

Transposition is another potential mechanism of translocation, which, if it occurs in neoplasms, is distinct from the RAG misrecognition mechanism. During transposition, the RAG complex has been shown to be capable of transposing signal ends from a V(D)J recombination event into a random location (1, 12, 17), and this has been conjectured to be a possible

* Corresponding author. Mailing address: Norris Comprehensive Cancer Center, Rm. 5428, University of Southern California, 1441 Eastlake Ave., MC9176, Los Angeles, CA 90033. Phone: (323) 865-0568. Fax: (323) 865-3019. E-mail: lieber@usc.edu.

† Supplemental material for this article may be found at http://mcb.asm.org/.

cause of genomic instability (33, 34). However, in known consistent translocations, such as at the bcl-2 gene, there is no transposition of heptamer/nonamer signals into the locus, nor are there consistent P nucleotides (short inverted repeats) that would be predicted if the RAG complex had carried out an integration/disintegration reaction (13, 24). There are only two instances thus far of likely transposition events in vivo, and these were in normal lymphocytic clones at the *hprt* locus rather than in neoplasms (25). Hence, it is less likely that transposition accounts for any of the well-characterized translocations (30).

The bcl-2 major breakpoint region (Mbr), involved in the t(14;18) translocation of nearly all follicular lymphomas, is the most important of all lymphoid cell translocations, because follicular lymphomas account for nearly half of all non-Hodgkin's lymphomas (3, 5, 13, 30, 42). The Mbr on chromosome 18 is in the 3′ untranslated region within exon 3 of the bcl-2 gene. The bcl-2 Mbr is distinctive among breakpoint regions (30). Nearly 75% of t(14;18) breakpoints are dispersed over a 150-bp region with relatively sharp boundaries (13, 42). Within the 150 bp, there are three peaks of breakage, each about 15 to 20 bp in size. The characteristic precision and frequency profile within the bcl-2 Mbr strongly suggest some strong local regional specificity to the bcl-2 Mbr (30).

Recently, we reported that the bcl-2 Mbr adopts a non-B form structure in vivo. This altered DNA structure can be recapitulated when the bcl-2 Mbr is present on a human minichromosome in vivo or on an *Escherichia coli* episome (31). The structure at the 150-bp bcl-2 Mbr contains distinctive regions of single-strandedness that correspond well to the regions of translocation frequency among patients. The structure formation can be recapitulated on different-length DNA fragments containing the bcl-2 Mbr and is dependent on Hoogsteen hydrogen bonding (28). Based on in vivo extrachromosomal substrate studies, we showed that RAGs are the nuclease responsible for the large majority of recombination events between the bcl-2 Mbr and the 12/23 signals. Finally, RAG nicking at the bcl-2 Mbr was demonstrated in vitro on a plasmid DNA substrate (31).

RAG-mediated nicks which do not proceed to DSBs can stimulate homologous recombination (16). It has been conjectured that the in vitro RAG nicking observed by us (31) might be an example of how RAG complex nicking (but not RAG-induced DSBs) might result in translocations (16). Here we report that, in fact, the RAG complex generates DSBs by creating independent nicks close to one another on the two strands at the bcl-2 Mbr. The creation of DSBs is dependent on the presence of a non-B DNA structure at the bcl-2 Mbr. A 3-bp mutation capable of destroying the non-B structure formation is also sufficient to abolish the RAG-induced DSB formation. A RAG active site mutant that lacks nicking activity is unable to produce the DSBs. We also show that the RAG complex can bind and cleave other non-B DNA structures containing single-stranded regions, indicating that the RAG complex is, indeed, a structure-specific nuclease. These findings highlight the novel properties of the RAG complex that are important not only for the t(14;18) chromosomal translocation, but also for the physiologic function of RAGs.

MATERIALS AND METHODS

Preparation of RAGs. Core murine GST-RAG1 (amino acids 330 to 1040) and GST-RAG2 (amino acids 1 to 383), MBP murine core RAG1 and RAG2, mutant RAG1 and core MBP-RAG2, core MBP-RAG1 and full-length MBP-RAG2, double-MBP murine core RAG1 and RAG2, or double-MBP murine core RAG1 binding mutant/double-MBP core RAG2 proteins were overexpressed in human 293T cells and purified as described earlier (38, 39, 44).

PCR amplification of shorter DNA fragments with and without the bcl-2 Mbr and gel shift assays. The methods used for PCR amplification of shorter DNA fragments and for gel shift assays are described in the "Methods" section of the supplemental material.

Detection of double-strand break formation on bcl-2 Mbr substrates by RAGs. Concentrations of RAGs (specified in the figure legends) were incubated with 10 ng of [γ-^{32}P]ATP end-labeled or [α-^{32}P]dCTP whole-body-labeled DNA fragments with bcl-2 Mbr containing the non-B DNA structure or with control fragments (248-bp bcl-2 Mbr mutant or 231-bp fragment from the ampicillin gene) in a reaction volume of 20 μl, containing buffer A (25 mM morpholinepropanesulfonic acid [MOPS], pH 7.0, 30 mM KCl, 30 mM potassium glutamate, and 5 mM $MgCl_2$ with 100 nM of HMG1). In the no-RAG control reaction mixtures, only the RAG reaction buffer or RAG reaction buffer plus HMG1 was used. Reaction mixtures were incubated at 37°C for 1 h and then terminated (by addition of 10 mM EDTA and 0.2% sodium dodecyl sulfate), followed by phenol chloroform extraction. The DNA was recovered by ethanol precipitation. The pellet was then resuspended in 20 μl of Tris-EDTA buffer and stored at −20°C. In some experiments, after the RAG cleavage reactions, the products were directly loaded onto a native polyacrylamide gel and the bands were resolved. The gel was dried, and signals were detected using a Molecular Dynamics PhosphorImager. In most of the experiments, the electrophoresis was carried out using a running buffer consisting of 1× Tris-borate-EDTA (TBE), pH 7.2, with 5 mM $MgCl_2$. In the experiment shown in Fig. 1D and E, below, the gel running buffer, 1× TBE, pH 8.4, was used.

Primer extension reactions were carried out by mixing the following on ice: 3 μl of DNA sample, 1× thermo polymerase buffer [10 mM KCl, 10 mM $(NH_4)_2SO_4$, 20 mM Tris HCl (pH 8.8), and 0.1% Triton X-100], 4 mM $MgSO_4$, 4 μM deoxynucleoside triphosphates, 0.25 μM end-labeled oligomers, and 0.4 U vent (exo-) polymerase (New England Biolabs, MA) after layering with mineral oil. Linear amplification primer extensions were carried out on a PCR machine (20 cycles) under the following conditions: 94°C for 3 min (1 cycle); 94°C for 45 seconds, 55°C for 45 seconds, and 75°C for 30 seconds (20 cycles); and final extension of 2 min. The reactions were then terminated by adding the stop dye. The reaction products were resolved on a 6% denaturing polyacrylamide gel. The gel was dried, and signals were detected as described above.

Preparation of symmetric bubble and heterologous loop structures. The symmetric bubble structure was created by annealing a [γ-^{32}P]ATP end-labeled 50-nucleotide (nt) oligomer YM231 with unlabeled 50-nt complementary oligomer YM21 (1:1 ratio) with slow annealing in 10 mM Tris (pH 8), 100 mM NaCl, or vice versa. A symmetric bubble structure with a G-C-rich region adjacent to the bubble (G-C clamp) was prepared by mixing SCR175 and SCR176. Oligomers SCR177 and -178 were mixed to create the symmetric bubble with an A-T region. Control duplex DNA of 50 bp in length was created by annealing SCR174 and YM21. A standard 12-signal was prepared by annealing KY28 and KY29. A standard 23-signal was prepared by annealing KY36 and KY37.

RAG cleavage on symmetric bubble and heterologous loop structures. The substrate DNA containing symmetric bubble or heterologous loops (10 nM) was incubated with core GST-RAG1 and RAG2 proteins (or core MBP-RAG1 and RAG2, core double-MBP-RAG1 and RAG2, or respective mutant versions of the RAGs, as indicated in the figure legends) in the presence of HMG1 for 1 h at 37°C in a buffer containing 25 mM MOPS, pH 7.0, 30 mM KCl, 30 mM potassium glutamate, and 5 mM $MgCl_2$ with 100 nM of HMG1. In control reactions, RAG reaction buffer plus HMG1 was used. Reactions were terminated by adding the loading dye containing formaldehyde. The reaction products were then resolved on a 15% denaturing polyacrylamide gel, and the signals were detected as described above. In some other cases where DNA double-strand breaks were detected, the reaction products were loaded onto a 15% native polyacrylamide gel and signals were detected as described above.

Electrophoretic mobility shift assay to detect RAG binding at the bcl-2 Mbr or on other non-B DNA structures. A 248-bp DNA fragment containing the bcl-2 Mbr, a subset of which forms the non-B DNA structure, was prepared as described above. Increasing concentrations of RAGs were incubated with 10 ng of [γ-^{32}P]ATP end-labeled DNA fragments with the bcl-2 Mbr containing the non-B DNA structure in a reaction volume of 15 μl, containing 25 mM MOPS, pH 7.0, 30 mM KCl, 30 mM potassium glutamate, and 5 mM $MgCl_2$ with 100 nM

of HMG1. In the no-RAG control reactions, only the RAG reaction buffer was used. A 45-bp double-stranded oligomer (1 μM) was added to the reaction mix as nonspecific DNA. Reaction mixtures were incubated at 37°C for 15 min, and the products were loaded immediately (after adding 30% glycerol) to a native polyacrylamide gel. After resolving the bands, the gel was dried, and signals were detected using a Molecular Dynamics PhosphorImager.

In studies where symmetric bubbles or heterologous loops were used for the RAG binding experiments, 10 nM of the substrate DNA ([γ-^{32}P]ATP end labeled) was incubated with RAGs (as mentioned in the figure legends) in the above-described RAG reaction buffer for 10 min at 37°C in the presence of nonspecific DNA (45-bp double-stranded oligomer; 1 μM). The products were resolved on a 6% native polyacrylamide gel, and radioactive signals were detected as described above.

Mutagenesis at the bcl-2 Mbr. The methods used for mutagenesis at the bcl-2 Mbr are described in the "Methods" section of the supplemental material.

P1 nuclease protection assay. For the P1 nuclease study, 10 nM symmetric bubble DNA substrate was incubated with P1 nuclease with and without pretreatment with RAG proteins (10 min at 37°C) in RAG reaction buffer (25 mM MOPS, pH 7.0, 30 mM KCl, 30 mM potassium glutamate, and 5 mM $MgCl_2$) at 37°C for 15 min. The reaction products were either mixed with 1× DNA dye and immediately loaded onto a native polyacrylamide gel (15%) or mixed with formamide-containing dye and loaded on a denaturing polyacrylamide gel (15%) as described above. P1 concentrations used for the study were 0.01 U, 0.1 U, 0.4 U, and 1 U, as described in the figure legends. The gel was dried and exposed to a phosphorimager screen, and images were obtained as described above.

RESULTS

RAGs induce double-strand breaks at the bcl-2 Mbr. We used bcl-2 Mbr-containing DNA fragments that can form the non-B DNA structure to further characterize RAG cleavage at the Mbr (28). In the present study, we have used PCR fragments of lengths of 248 and 339 bp (Fig. 1A). The [γ-^{32}P]ATP end-labeled DNA fragments containing the bcl-2 Mbr were permitted to form the structure by incubation in Mg^{2+} buffer (see Materials and Methods) (31). These DNA fragments were then used for RAG cleavage experiments. The RAG proteins and the non-B DNA substrate were incubated at 37°C for 1 h, and the reaction products were then resolved on native polyacrylamide gel electrophoresis (PAGE) gels (either pH 7.2 or pH 8.4). In the presence of RAGs, the 248-bp fragment was cleaved to form two new bands. One band runs at approximately 180 bp, which is clearly visible, and the other at approximately 50 bp, which is not readily visible at the exposure shown (Fig. 1B) but is visible on a native gel run at pH 8.4 (Fig. 1D). (Based on denaturing gel electrophoresis of the top and bottom strands run independently, it appears that the actual length of the 50-bp fragment observed is ~70 bp [see below]. It is also important to note that DNA fragments containing non-B DNA structures may run slightly aberrantly on native gels relative to markers of duplex length.) Because we resolved the products on native gels, this band can be generated only if there is a DSB on the DNA. A single nick would not generate a new band on a native gel (nor would it generate one at this position). Another interesting feature of this study is that the break location matches with the non-B structure-forming region (upstream of peak 1) that was identified in the oligomer annealing experiments described previously (28, 31). Thus, these results indicate that the RAGs are capable of generating DSBs at the bcl-2 Mbr in vitro, consistent with the in vivo RAG dependence (31).

We also tested the 339-bp bcl-2 Mbr fragment for RAG-induced DSB formation. The results showed that in the presence of the RAGs, two cleavage bands were readily visible (Fig. 1C, pH 7.2 gel, and E, pH 8.4 gel). One cleavage band is at 130 to 135 bp, and the other is at 180 to 205 bp (Fig. 1C and E). These two bands indicate a single double-strand break within the region of non-B structure formation defined in a previous study of this fragment (in this fragment, the non-B structure formation occurs at peak III and downstream of peak I) (28). This further confirms the results obtained from the 248-bp fragment analysis.

Double-strand breaks caused by RAGs require the non-B DNA structure at the bcl-2 Mbr. In our previous report, we could independently show that the bcl-2 Mbr is capable of adopting a non-B DNA structure (31). By transfection experiments and RAG cleavage on plasmid DNA, we could also show that RAGs could be the enzyme responsible for the bcl-2 Mbr cleavage. However, we were unable to directly correlate the RAG cleavage to the structure formation, though the circumstantial evidence was compelling. That is, we did not show that the subset of DNA assuming the non-B DNA conformation was the same subset of DNA being cut by the RAG complex.

Here, we were able to test this association directly. The addition of an increasing concentration of RAGs does not cause any reduction in the quantity of the 248-bp duplex DNA band (Fig. 1B). However, for the shifted band (non-B DNA), there is a proportional reduction in proportion to the RAG complex concentration (Fig. 1B). This suggests that the RAG cleavage products that we observed result primarily from the shifted species rather than from the duplex DNA. A similar reduction in the quantity of shifted species was also observed in the case of the 339-bp fragment (Fig. 1C). These results indicate that the RAG complex recognizes the non-B DNA region and induces the DSB.

We have further studied the positions of the RAG cleavage on the top and bottom strands by performing primer extension reactions using end-labeled primers specifically for those strands (see Fig. S1 in the supplemental material). Then, the products were resolved on a denaturing polyacrylamide gel. On the top strand of the 248-bp fragment, there was a new band generated at approximately 180 bp, which is located upstream of peak I (Fig. 2A; see also Fig. S2 in the supplemental material), which is where we have documented long single-stranded regions due to non-B DNA structure by a variety of other methods (28, 31). On the bottom strand, two bands are visible, one at approximately 70 bp (a cluster of bands) and another one at 145 bp (Fig. 2A; see also Fig. S2 in the supplemental material). The 70-bp band is due to a nick upstream of peak I. These results suggest that the 180-bp band observed on the native gel described above (Fig. 2A; see also Fig. S2 in the supplemental material) is due to two RAG nicking events, one on the top and a second one on the bottom strand. Further, these results raise the possibility that the DSB generated may be staggered due to independent nicks that are not directly across from one another. The second band observed on the bottom strand at the position for nt 145 on the denaturing gel is most likely due to a nick at a CAC sequence located close to the 5′ end of peak II (Fig. 2A; see also Fig. S2 in the supplemental material). However, in this case, it is not converted to a DSB, in contrast to the break upstream of peak I, where the non-B DNA structure exists. This explains the reason for the absence of any band corresponding to this position on the

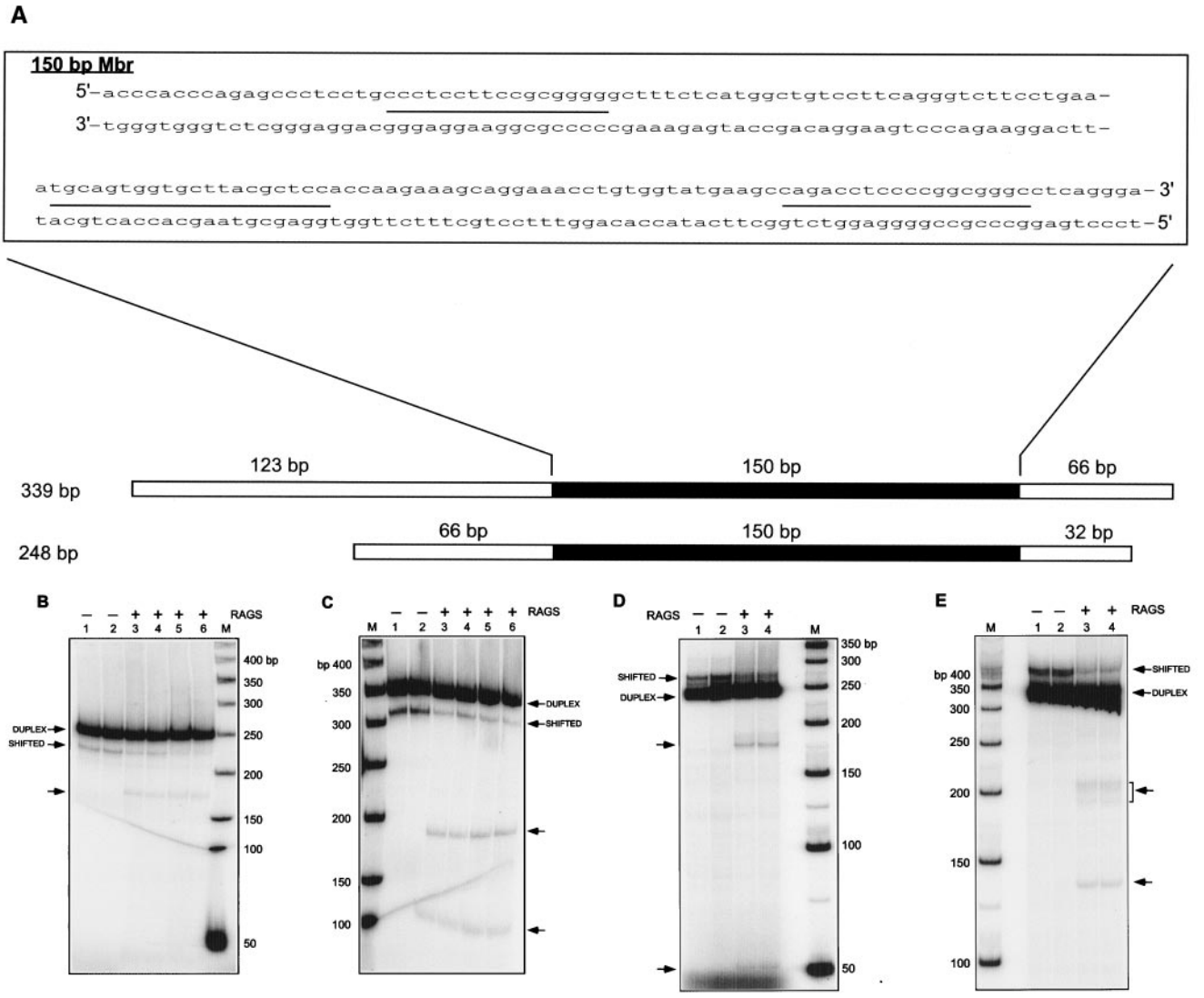

FIG. 1. RAG-induced double-strand break formation on DNA fragments containing the bcl-2 Mbr. A. Location of the bcl-2 Mbr on the 248-bp and 339-bp DNA fragments with respect to the surrounding sequences. The DNA surrounding the Mbr is represented as an open box, and the 150-bp Mbr is indicated in solid black. The sequence of the Mbr is shown in a separate window, divided into two rows, with the sequence continuation represented by a hyphen. The three breakpoint peaks are designated as lines between the two strands, peak I being in the top row and peaks II (left) and III (right) in the bottom row. B and C. Increasing concentrations of RAG protein complex were incubated with the bcl-2 Mbr fragment containing the non-B conformation for 1 h at 37°C in buffer A. Immediately after the incubation, the products were resolved on a 6% native polyacrylamide gel using 1× TBE (pH 7.2) in the presence of $MgCl_2$. RAG-induced DSB formation on a [γ-^{32}P]ATP end-labeled 248-bp (B) or 339-bp (C) bcl-2 Mbr fragment is shown. In both panels, the lanes are as follows: lanes 1 and 2, DNA fragments containing the bcl-2 Mbr non-B structure treated with 0 ng RAGs; lanes 3 and 4, 50 ng RAGs; lanes 5 and 6, 100 ng RAGs; lane M, 50-bp ladder. D and E. A 100-ng aliquot of RAG protein complex was incubated with the bcl-2 Mbr fragment containing the non-B conformation for 1 h at 37°C in buffer A. Immediately after the incubation, the products were resolved on a 6% native polyacrylamide gel using 1× TBE (pH 8.4). RAG-induced DSB formation on a [α-^{32}P]dCTP body-labeled 248-bp (D) or 339-bp (E) bcl-2 Mbr fragment is shown. In both panels, the lanes are as follows: lanes 1 and 2, DNA fragments containing the bcl-2 Mbr non-B structure treated without RAGs; lanes 3 and 4, bcl-2 Mbr fragments treated with RAGs; lane M, 50-bp ladder. In panels B to E, each sample was prepared in duplicate and loaded in duplicate lanes. In these panels the duplex DNA and shifted band containing the non-B form DNA are indicated. The new bands generated due to RAG cutting are indicated by arrows.

native gel (Fig. 1B). We also found a band of about 100 nt in length, which is most likely due to RAG cleavage on the bottom strand (upon denaturation of the DNA sample after RAG cleavage) (Fig. 2A; see also Fig. S2 in the supplemental material).

A similar study was carried out on the 339-bp fragment, where non-B structure formation occurred at peak III and downstream of peak I (28) (Fig. 2B). In this case also, the break site on the top strand and the bottom strand matched the region of structure formation at peak I (see Fig. S3 in the supplemental material). The DSB might result from one nick on the top strand and one nick on the bottom strand (Fig. 2B), or the DSB might result from one nick on the bottom strand of peak I (Fig. 2B) and one on the top strand at peak II (Fig. 2B); the single-strandedness in the non-B structure between peaks

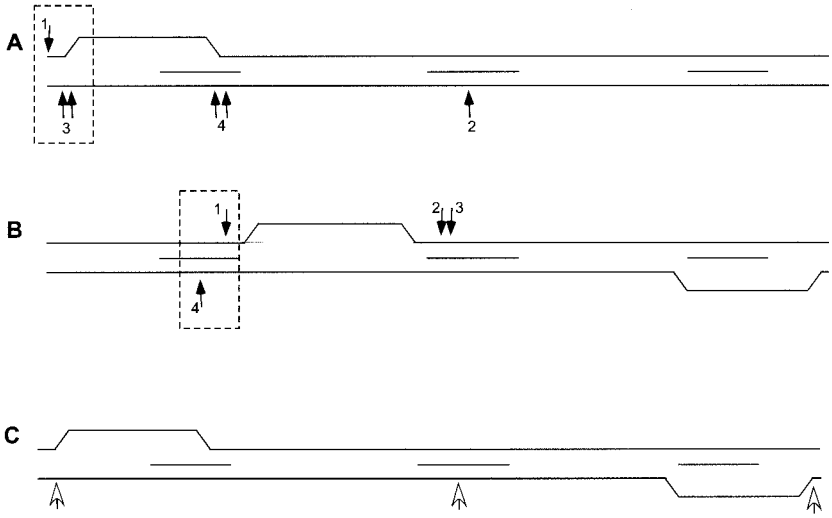

FIG. 2. RAG cleavage sites with respect to the location of the structure formation at the bcl-2 Mbr. In all panels, the 150-bp Mbr is depicted and peaks I, II, and III are indicated by short horizontal lines between the top and bottom strands (represented by the long lines). The arrows pointing downward refer to RAG nicks on the top strand, and arrows pointing upward refer to RAG nicks on the bottom strand. The positions of RAG cleavage shown are determined on the basis of results obtained from both native and denaturing PAGE. Dashed boxes indicate combinations of top and bottom strand nicks that are most likely responsible for the double-strand breaks seen on the corresponding native gels in Fig. 1. A. RAG cleavage on a 248-bp Mbr-containing fragment. Here, the non-B structure formation is upstream of peak I and is represented as the nonduplex region. The actual nature of the non-B structure is not assumed here, but it is not the simple bubble depicted; this is just the simplest DNA deviation for illustrative purposes. The numbered arrows correspond to the numbered cleavage bands in Fig. S2 of the supplemental material. B. RAG cleavage on a 339-bp Mbr-containing fragment. Here, the structure formation is downstream of peak I and peak III. The numbered arrows correspond to the numbered cleavage bands in Fig. S3 in the supplemental material. C. Sites of RAG nicking on plasmid DNA containing the bcl-2 Mbr. Here, RAG nicking sites are detected by primer extension, indicated by open arrows. See the legend of Fig. S4 in the supplemental material for additional details.

I and II would then contribute to the DSB outcome. These results further suggest that the RAG-induced DSBs at the bcl-2 Mbr can be correlated with the non-B structure formed at the Mbr. However, in this case we did not find any RAG cleavage at peak III (Fig. 2B), despite the fact that in some cases structure formation was detectable at peak III (see Discussion).

A 3-bp mutation in the Mbr abolishes the RAG-induced double-strand DNA breaks. We wondered whether the RAG-induced DSB formation was affected by a 3-bp mutation at the bcl-2 Mbr. The 3-bp mutation involves an exchange of three C residues on the top strand with the complementary three G residues on the bottom strand upstream of peak I (Fig. 3A). The mutant PCR fragment (248 bp) was PCR amplified, end labeled, and incubated in Mg^{2+}-containing buffer, as described earlier. This substrate was then subjected to RAG incubation, and the products were resolved by native PAGE (pH 7.2). The results showed that, compared to the normal bcl-2 Mbr fragment (248 bp), there was no shifted band, suggesting no structure formation (Fig. 3B, compare lanes 1 and 2 with lanes 5 and 6). The 3-bp mutation is upstream of peak I, precisely where the structure formation takes place on the 248-bp fragment (Fig. 3A).

Interestingly, in contrast to the 248-bp Mbr fragment, in the case of the 248-bp mutant fragment there are no new bands created when it is treated with the RAG complex (Fig. 3B, compare lanes 3 and 4 with lanes 7 and 8). This suggests that structure formation is prerequisite for DSB formation by the RAGs. Similarly, when a control DNA fragment from the β-lactamase gene, lacking the non-B DNA structure (no shifted species in this case) was subjected to RAG treatment, we could not see any new RAG-induced cleavage products (data not shown). This strongly confirms the above finding that the RAG complex recognizes the non-B DNA structure, rather than any cryptic heptamer/nonamer signal-like sequence present at that region. Hence, there is no misrecognition by the RAGs at the bcl-2 Mbr sequence. The cleavage is entirely dependent on the non-B conformation of that sequence and not on the duplex conformation.

Mutant RAGs are unable to induce double-strand DNA breaks. We further tested RAG cleavage specificity by replacing the RAGs with catalytically inactive mutant RAGs (mutant RAG1 and core RAG2). Although the core RAG1 and -2 are capable of inducing DSBs, the mutant RAGs (mutant RAG1/core RAG2) are unable to induce these bands in the 248-bp fragment or the 339-bp fragment when the same conditions are used to perform the RAG cleavage assay (Fig. 4). This shows that the endonuclease activity is due to the RAGs and not due to any contaminating nuclease present in the RAG preparation.

Recently, it was shown that full-length RAG2, in combination with core RAG1, has reduced in vitro RAG transposition activity relative to core RAG1 and -2 proteins (6, 38, 40). Transposition of signal ends into the bcl-2 Mbr has never been observed. Nevertheless, we tested whether the core RAG1/full-length RAG2 behave similarly to the core RAG complex. For this purpose, we incubated the 248-bp or the 339-bp fragments with full-length RAGs. Results showed that there is no differ-

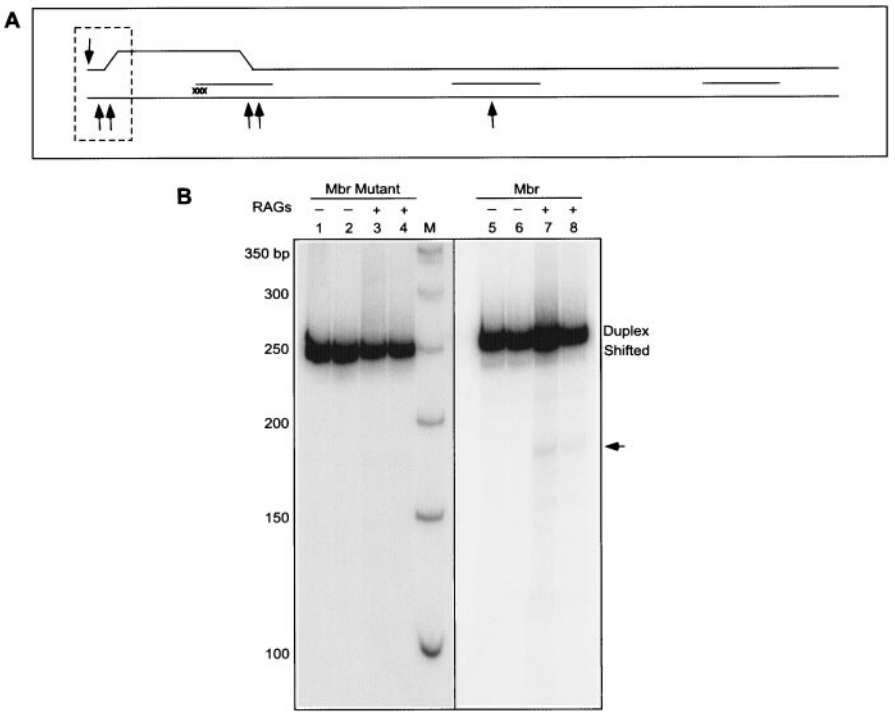

FIG. 3. RAG cleavage on a 3-bp bcl-2 Mbr mutant. A. The Mbr portion of the 248-bp fragment containing a CCC↔ GGG exchange between the top strand and bottom strands is shown. Note that the Mbr portion is only 150 bp and, hence, the 248-bp fragment is longer than shown in the diagram. The position of the 3-nt exchange is indicated by "xxx." The region of structure formation is marked as in Fig. 2A. For other details, refer to Fig. 2. B. The 248-bp PCR fragment containing the mutated bcl-2 Mbr or the wild-type Mbr was then end-labeled and studied in the presence or absence of the RAG complex. RAG incubation products were then loaded onto a native PAGE. Lane M is the marker. The positions of the duplex DNA and shifted band containing the non-B DNA are indicated. The new band generated by RAG cleavage is indicated by an arrow. Each sample was prepared in duplicate and loaded in duplicate lanes. Both panels of the figure are derived from the same gel.

ence in Mbr nicking pattern or efficiency resulting from the activity of core RAG1/core RAG2 relative to core RAG1/full-length RAG2 (Fig. 4A and B). Along with the fact that there is no transposition observed here, this further weighs against the involvement of some variant transposition mechanism in the generation of the DSBs at the bcl-2 Mbr. Therefore, our study clearly demonstrates that the RAGs recognize the stable non-B DNA structure present at the bcl-2 Mbr to induce the DSBs.

Our studies using supercoiled and linear plasmid DNA substrates also indicated that RAG cleavage is influenced by the presence of the non-B DNA structure (see the Results section in the supplemental material).

Test for RAG binding at the bcl-2 Mbr. Since we could observe the RAG-induced double-strand break formation at the bcl-2 Mbr, it is clear that the RAG complex must bind to the DNA. We wondered whether we could directly detect this RAG binding step at the bcl-2 Mbr. In order to perform this experiment, we incubated increasing concentrations of RAGs with a 248-bp DNA ([γ-^{32}P]ATP end-labeled) fragment containing the bcl-2 Mbr structure in RAG reaction buffer for 15 min at 37°C. The products were resolved on a 5% native polyacrylamide gel. Results did not show any detectable level of RAG binding to the bcl-2 Mbr even after multiple trials (data not shown). This suggests two possibilities. First, the RAG binding may not be stable at this site. RAGs might be binding the structure and releasing from it in rapid equilibrium. A second possibility is that RAG binding might be limited only to a small percentage of the molecules that contain the structure at a given time. This means out of the 10 to 15% of the DNA molecules with the non-B structure, RAGs may bind only to a subset of these molecules, resulting in an undetectably low percentage of molecules manifesting any binding.

The RAG complex cleaves other non-B DNA structures. The results thus far indicate that RAGs induce DSBs at bcl-2 Mbr only when a non-B DNA structure exists. Besmer et al. (4) showed that RAGs are capable of cleaving the hairpins in Mn^{2+} buffer and, subsequently, a weak RAG cleavage activity (in Mg^{2+} buffer) was detected on a hairpin substrate (37). What other single-strand–double-strand structural transitions might be cut by RAGs? Here, we further tested the RAG cleavage activity on symmetric bubbles and heterologous loops under physiological conditions (Fig. 5). In order to perform this, one of the strands was [γ-^{32}P]ATP end labeled and annealed with the complementary strand to create the structure (either a symmetric bubble or a heterologous loop) (see Materials and Methods) (Fig. 5). The end-labeled DNA was then incubated with increasing concentrations of RAGs at 37°C for 1 h. The products were then resolved by denaturing 15% PAGE.

The results show that several new bands are visible in the presence of the RAGs for both the symmetric bubble structures and heterologous loop substrates (Fig. 5 and 6). The pattern of bands observed indicates that cleavage occurs at

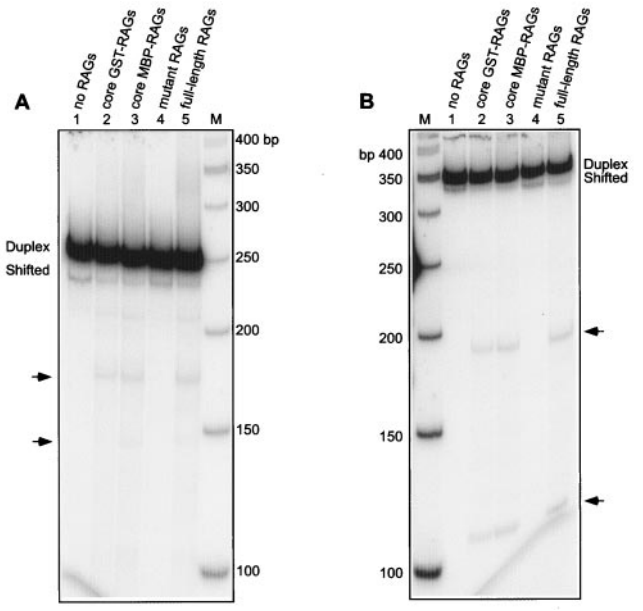

FIG. 4. Comparison of core, full-length, and mutant RAG-induced DSB formation at the bcl-2 Mbr. A 248-bp (A) or 339-bp (B) DNA fragment of the bcl-2 Mbr containing non-B structure was incubated with different RAG preparations (see below). The products were resolved on a 6% PAGE. (See Fig. 1 legend for details.) In both panels A and B, the descriptions of the lanes are as follows: RAG-induced DSB formation with no RAG protein (lane 1); core GST-RAGs (stands for core GST-RAG1/core GST-RAG2) (lane 2); core MBP-RAGs (stands for core MBP-RAG1/core MBP-RAG2) (lane 3); mutant RAGs (stands for mutant RAG1/core MBP-RAG2) (lane 4); full-length RAGs (stands for core MBP-RAG1/full-length MBP-RAG2) (lane 5). The RAG-sensitive regions are indicated by arrows. Lane M, molecular weight markers. The faint band at 210 bp in panel A is present in all lanes.

specific regions. The plotting of the RAG cleavage sites shows that RAG nicking mostly occurs at multiple locations in the adjacent double-stranded portion (Fig. 5 and 6). Among the different RAG-sensitive sites, we found that the nucleotides at the junction of single- and double-stranded DNA are highly sensitive to RAG cleavage on a symmetric bubble structure (Fig. 5A and 6, lanes 8 and 9). Very rarely, we found a single cut site near the middle of the single-stranded region in the case of the symmetric bubble structures (Fig. 6). These results show that RAGs are able to nick both symmetrical bubble structures and heterologous loop structures.

In addition to both symmetrical bubble structures and heterologous loop structures, we also found that the RAG complex is able to cleave stem-loop structures (data not shown). The loop region tested was 10 nt in length. In this case, the location of RAG cleavage is within the duplex DNA adjacent to a single-strand–double-strand transition.

RAG cleavage requires the presence of the non-B DNA structure. Since we detected RAG nicking on the bcl-2 non-B DNA structure, the symmetric bubble structure, and the heterologous loop structures, we designed double-stranded DNA of the same length as the symmetric bubbles. Except at the bubble region, the sequence was identical to the duplex. RAG cleavage experiments showed that there is no new band generated by RAG digestion (Fig. 6, compare lanes 5 and 6). This suggests that unusual DNA structures are a prerequisite for RAG cleavage at sites that are not similar to V(D)J recombination signal sequences. Above, we have also seen that RAG cleavage does not occur when a 3-bp alteration destroys the structure at the bcl-2 Mbr (Fig. 3). In an earlier study Santagata et al. (1999) also observed only background nicking when they used double-stranded DNA for RAG cleavage experiments. We also used two independent single-stranded DNAs (50 nt) of the same sequence to test for RAG nicking (Fig. 6, lanes 1 to 4). We did not find any RAG nicking at one of the single-stranded DNA substrates (Fig. 6, compare lanes 3 and 4). However, in the second single-stranded DNA substrate, we did find some background nicking (Fig. 6, compare lanes 1 and 2). Since it is a 50-nt-long single-stranded DNA, it is possible that the DNA may fold back on itself to form a base-paired or secondary structure, and this may explain the RAG sensitivity observed in this substrate.

We also found a similar pattern of nicking when GST-core RAGs were replaced with MBP-core RAGs, under otherwise similar reaction conditions (Fig. 6, compare lanes 8 and 9). This indicates that the RAG nicking observed due to the glutathione *S*-transferase (GST)–RAG preparation on these DNA structures is attributable to the RAGs themselves and is not an artifact. In addition, when we replaced the MBP-core RAGs with MBP-core catalytic mutant RAG1 and MBP-core RAG2, we did not find any RAG cleavage (Fig. 6, compare lanes 9 and 10). This suggests that the active site of RAG1 is essential for the RAG nicking on altered DNA structures.

The RAG cleavage on symmetric bubble structures and heterologous loops predominantly occurs adjacent to double-stranded DNA. Therefore, we wondered whether the bubble region (10 nt in length) can expand due to breathing at the edges and whether that could be the reason for the sensitivity at the adjacent double-stranded DNA. We synthesized two variations of the symmetric bubble. In one case, the sequence on double-stranded DNA close to the single-stranded DNA–dsDNA junction was replaced with G-C-rich sequences (G-C clamp) and in the other case with A-T-rich sequences. RAG cleavage experiments were performed using these new substrates under the same conditions as described above. Results showed that, similar to the earlier experiments, these bubble structures are also cleavable by RAGs (Fig. 6, lanes 11 to 14). There was no significant difference in the cleavage pattern when random sequence (Fig. 5A), G-C-clamped (Fig. 6, lanes 11 and 12), or A-T-rich (Fig. 6, lanes 13 and 14) symmetric bubble substrates were used.

RAGs induce double-strand breaks on symmetric bubble and heterologous loop structures. Since we have seen RAG nicking on one of the strands of symmetrical bubble or heterologous loop structures, we tested the RAG sensitivity on the second strand. Such neighboring nicks on both strands collectively can lead to a DSB, as we have seen in the case of the bcl-2 Mbr. In order to perform such an experiment, we end labeled ([γ-^{32}P]ATP end labeled) either on the top or bottom strands of the symmetrical bubble or heterologous loop structures and annealed with respective unlabeled antiparallel strands. Results showed that upon incubation with the RAG complex, we detected RAG nicking on both the top and bottom strands in symmetric bubble structures as well as heterologous loop structures (Fig. 7A). In the case of the heterologous

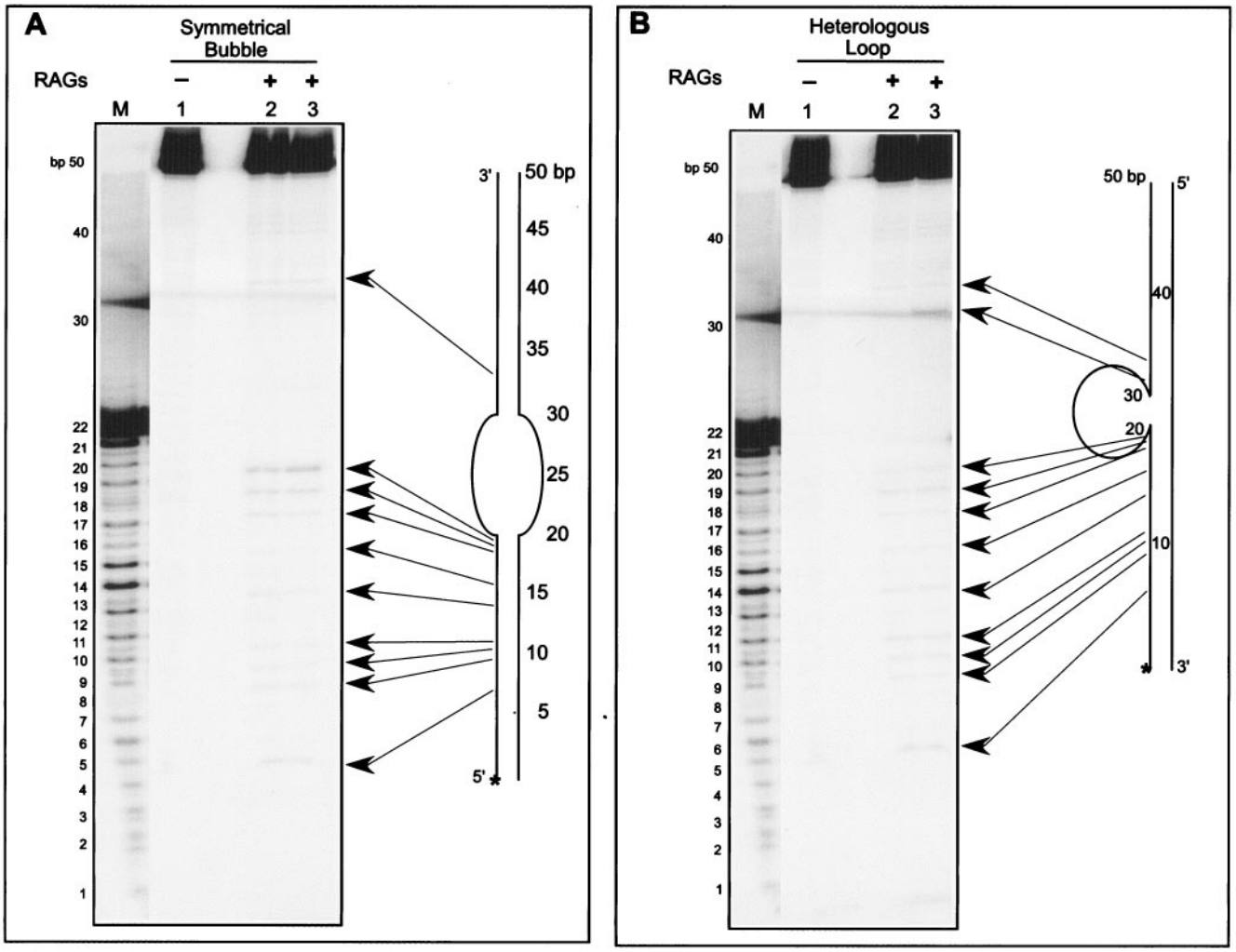

FIG. 5. RAG cleavage on a DNA bubble and a heterologous loop. Increasing concentrations of RAG1 and RAG2 complexes were incubated with a [γ-^{32}P]ATP end-labeled 50-bp ds oligomers containing a symmetric bubble structure (A) or a heterologous loop structure (B) for 1 h at 37°C in buffer A. Afterwards, the cleavage products were resolved on a 15% denaturing polyacrylamide gel. In both panels A and B, the lanes are as follows: 1, 50-bp DNA containing the DNA treated with 0 ng RAGs; lane 2, 50 ng RAGs; lane 3, 100 ng RAGs; lane M, 50-bp ladder. In both panels, the sites of RAG cleavage with respect to the corresponding structure are indicated by long arrows. Corresponding nucleotide positions in the structure are marked. The [γ-^{32}P]ATP-labeled 5′ end of the structure is indicated with an asterisk. Intervening lanes between the marker lane and lanes 1 to 3 have been removed. The band in panel B, lane 3, at ~32 bp is obscured somewhat by a diffuse band that is present across the gel (even in the blank lane between lanes 1 and 2) just below that position.

loops, we found RAG nicking on both sides of the bubble structure on one of the strands (Fig. 7A, lane 6). We found such a pattern of cleavage in the case of the symmetric bubble structure as well (Fig. 5A, lanes 2 and 3). In this case also, the nicking was restricted to the neighboring double-stranded region of the single-strand–double-strand transitions (Fig. 7A and B). These results show that RAGs nick on both top and bottom strands of the symmetric bubble or heterologous loop structures. The RAG nicking observed on the top and bottom strands indicates that even in these cases RAG nicking will lead to DNA DSB formation.

In order to further detect the DSB formation by RAGs on a symmetric bubble and heterologous loop structures, we performed RAG cleavage reactions as described earlier. The products were resolved on a native polyacrylamide gel (15%) after the DNA was organically extracted and purified. As important controls, RAGs do not generate any DSBs on dsDNA (see Fig. S5 in the supplemental material [compare lanes 3 and 4]). It is important to point out that in all three cases (dsDNA and symmetric bubble and heterologous loop structures) the length of the DNA is 50 bp. The mobilities of all three different DNA configurations are varied, because the DNA is run on a native gel (see Fig. S5, lanes 3 to 8, in the supplemental material).

The results showed that in the case of both the symmetric bubble structure and the heterologous loop structure, we found new bands generated from RAG cleavage (see Fig. S5 in the supplemental material, lanes 6 and 8). Based on the molecular weight markers, it appears that the bands indicated are due to the formation of DSBs (see Fig. S5, lanes 5 to 8, in the

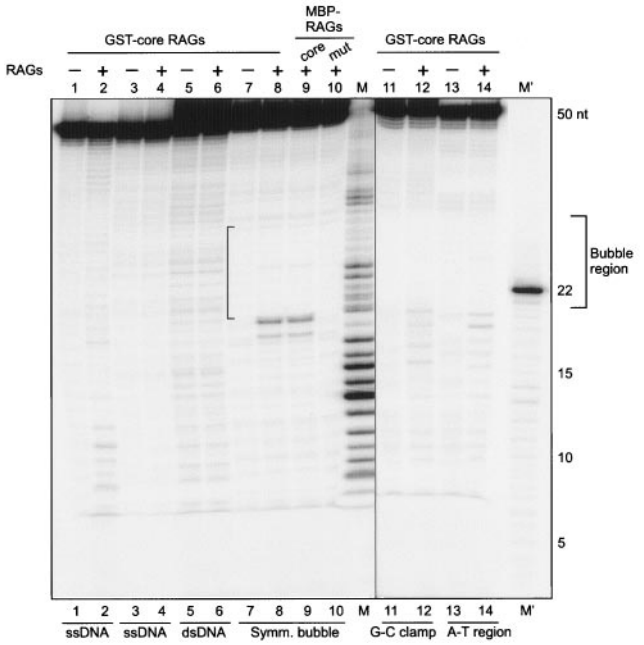

FIG. 6. Comparison of RAG cleavage on different symmetric bubble structures versus double- and single-stranded DNA substrates. RAG complexes (100 ng) were incubated with a [γ-^{32}P]ATP end-labeled 50-bp double-stranded DNA, 50-nt single-stranded DNA, or a symmetric bubble structure (see bottom of gel) for 1 h at 37°C in buffer A. The cleavage products were resolved on a 15% denaturing polyacrylamide gel. Two different oligomers, SCR174 (lanes 1 and 2) or YM21 (lanes 3 and 4) were used. A 50-bp double-stranded DNA was prepared by annealing YM21 and SCR 174 (lanes 5 and 6). Symmetric bubbles were prepared as described in Materials and Methods (lanes 7 to 10). The position of the bubble is indicated by the bracket. Symmetric bubbles containing G-C clamps were prepared by annealing SCR175 and SCR176 (lanes 11 and 12). Bubbles with A-T regions were prepared by annealing SCR177 and SCR178 (lanes 13 and 14). In all cases except lanes 9 and 10, core GST-RAG proteins were used. In the case of lane 9, core MBP-RAG1 and core MBP-RAG2 were used. For lane 10, the core MBP-RAG1 active site mutant and core MBP-RAG2 were used.

supplemental material). These studies, in conjunction with the above studies, indicate that independent RAG nicks may result in DSBs.

In addition to the double-strand break products (see Fig. S5 in the supplemental material), there is an additional band formed after RAG treatment of the symmetric bubble and of the heterologous loop (Fig. S5, lanes 6 and 8), which we interpret to be nicked forms of the loops, based on the following. We used synthetic prenicked symmetric bubble structures to determine where such nicked bubble structures migrate (see Fig. S6, lane 5, in the supplemental material). It should be noted that we do not know the precise location of the nick near the edge of the bubble; hence, the mobility of this control nicked symmetric bubble is not precisely the same as the actual RAG-generated nicked symmetric bubble (see Fig. S6, lane 4, in the supplemental material).

These results suggest that, similar to the RAG-induced DSBs observed at the non-B DNA structure of the bcl-2 Mbr, RAGs may induce DSBs on other non-B DNA structures.

RAGs bind to the symmetric bubble and heterologous loop structures. Since RAGs are able to cleave the symmetric bubble and heterologous loop structures, we tested whether RAGs are able to bind to these structures. To test this, DNA substrates containing symmetric bubble or heterologous loop structures were prepared as described above. In order to perform this experiment, we incubated increasing concentrations of RAGs with 50-bp DNA symmetric bubble and heterologous loop structures ([γ-^{32}P]ATP end labeled) in RAG reaction buffer in the presence of nonspecific DNA for 10 min at 37°C. The products were resolved on a 6% native polyacrylamide gel. Results showed that RAGs are able to bind to the symmetric bubble structure, resulting in a new high-molecular-weight band (Fig. 8, lanes 1 to 6; Fig. 9A, compare lanes 5 and 6). The shift in the band is increased according to the increase in the protein concentration (Fig. 8, lanes 1 to 6). There is also another new band generated just above the position of the substrate DNA (Fig. 8, lanes 1 to 6). It appears that this band is due to a nicking on one strand of the bubble structure by RAGs (see below). In the case of the heterologous loop structure, the RAG binding is weak, visible only at higher RAG concentrations (Fig. 8, lanes 7 to 12). However, in both cases the position of the shifted band due to the RAG binding remained the same.

Further studies showed that RAG binding is very weak or nonexistent when a 50-nt single-stranded DNA is incubated with RAGs (Fig. 9A, lanes 1 and 2). There was no binding of RAGs to a double-stranded DNA (derived from the same sequence as the symmetric bubble) (Fig. 9A, compare lanes 3 and 4). When a 50-bp duplex DNA containing a standard 12-signal was incubated with equal amounts of RAGs, we found a stronger RAG binding compared to the symmetric bubble structure (Fig. 9A, compare lanes 6 and 8). The RAG complex binds more efficiently to a 50-bp duplex DNA containing a standard 23-signal than to a symmetric bubble structure (Fig. 9A, compare lanes 6 and 10). These results indicate that though RAG binding occurs at the symmetric bubble structures, the efficiency is weaker compared to a standard V(D)J recombination signal. However, we also found that nucleotide alterations in a standard 12-signal sequence can drastically reduce the RAG binding efficiency (compare lane 8 of Fig. 9A with lane 2 of B).

RAG binding studies on symmetric bubble structures using MBP-core RAGs yielded similar results as that of the GST-core RAGs (Fig. 9B, compare lanes 4 and 5). The difference in the position of the shifted band upon RAG binding could be attributed to the difference in the length of the GST tag versus the MBP tag. Further, in the case of MBP-RAGs we found an additional shifted band just above the first shifted band. Earlier RAG binding studies using the same MBP-RAGs on V(D)J recombination signal also showed a similar pattern of RAG binding (38, 39). In those studies, it was shown that the first shifted band was attributable to the binding of two RAG1 molecules and one RAG2 molecule ([RAG1]2 [RAG2]1, also known as SC1). The second shifted band is due to the binding of two RAG1 and two RAG2 molecules ([RAG1]2 [RAG2]2, also known as SC2).

Interestingly, even with MBP-RAGs, we found the same new band that we observed for the GST-core RAG experiment, just above the substrate DNA position, probably due to

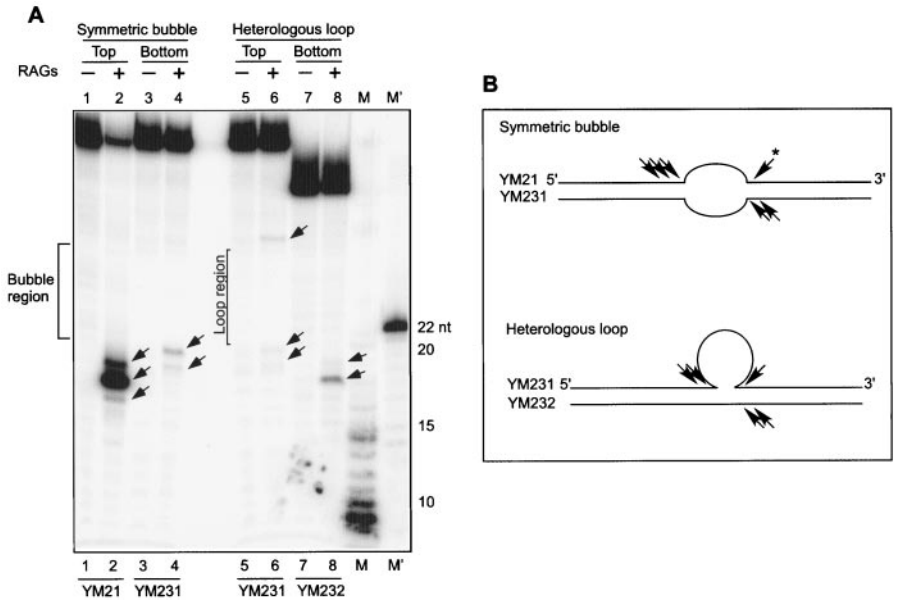

FIG. 7. RAGs induce double-strand breaks on symmetric bubble and heterologous loop structures. A. Gel showing RAG-induced nicks on both strands of the symmetric bubble and heterologous loop structures. Core GST-RAG proteins (100 ng) were incubated with a [γ-^{32}P]ATP end-labeled 50-bp symmetric bubble structure or heterologous loop structure for 1 h at 37°C. Afterwards, the cleavage products were resolved on a 15% denaturing polyacrylamide gel. In order to detect the RAG nicking at the top or bottom strand, the respective strand of the heterologous loop or symmetric bubble structure was [γ-^{32}P]ATP end-labeled and used for RAG cleavage. M and M′ stand for molecular weight markers. The bubble region of the symmetric bubble is demarcated. The loop region of the top strand of the heterologous loop is demarcated; note that this does not apply to the bottom strand. RAG nicking positions are indicted by arrows. B. Schematic presentation of RAG nicking positions on symmetric bubble and heterologous loop structures. Oligomers used for making the structures are indicated. RAG nicking positions on both strands are indicted by an arrowhead. The asterisk next to the arrowhead indicates that this cleavage is noted on a different gel (Fig. 5).

partially cleaved substrate DNA. Further, when we performed the RAG binding studies using an MBP-core RAG1 active site mutant–MBP-core RAG2 complex, we found very interesting results. RAG binding persisted, though the efficiency was reduced. More importantly, the band just above the substrate DNA level was not found (Fig. 9B, compare lanes 5 and 6). An active site mutant abolishes the RAG nicking but not the binding (38). The band just above the substrate DNA level is the result of the RAG complex nicking on one strand as described above (see Fig. S5 and S6 in the supplemental material). When the GST-core RAGs were replaced with double MBP-core RAG1 and MBP-core-RAG2, RAG binding remained comparable, but the efficiency was reduced (Fig. 9C, lanes 2 and 3). Here again, the shifted position of the RAG-bound band could be attributed to the difference in the length of GST and double-MBP tags. In this case also, the two shifted bands can be explained as described above. However, in the presence of the double MBP-core RAG1 binding mutant (the nonamer binding domain is mutated) and double MBP-core RAG2 proteins, RAG binding is completely abolished (Fig. 9C, compare lanes 3 and 4). In addition, the band just above the substrate DNA level (due to RAG nicking) is also absent. These results indicate that RAGs are able to bind the symmetrical bubble structures efficiently relative to standard V(D)J recombination signals. Mutation in the RAG1 catalytic site does not affect the binding; however, a mutation in the binding domain of RAG1 does destroy the RAG complex binding to symmetrical bubble structures.

RAG binding appears to cover at least some of the single-stranded region of the altered DNA structure. We used a P1 nuclease protection assay to determine whether the RAG binding occurs at and requires the double-stranded versus the single-stranded portions of the symmetric bubble. The RAG complex does not bind significantly at duplex DNA that lacks heptamer/nonamer sequences (38). We preincubated the substrate DNA (50 bp) containing the symmetric bubble ([γ-^{32}P]ATP end labeled) with RAG proteins for 10 min in RAG reaction buffer at 37°C. Then, we incubated increasing concentrations of P1 nuclease (single-strand nuclease) with bubble structures in the same buffer for 15 min at 37°C. Increasing concentrations of P1 nuclease treatment were carried out as controls on DNA substrates containing symmetric bubbles that were not incubated with the RAGs, and the products were resolved on a native 15% PAGE (Fig. 10A).

Results showed that a P1 nuclease concentration of 0.01 U is sufficient to digest the symmetric bubble structure, causing the disappearance of the 50-bp substrate DNA band (Fig. 10A, compare lanes 1 and 2). In this case, as a result of the P1 digestion, at the single-stranded region of the bubble structure, a new smear at the 20- to 30-bp position is visible. A further increase in the P1 concentration resulted in total digest of the substrate DNA and its products (Fig. 10A, lanes 3 to 5). When similar concentrations of P1 nuclease were used to treat the symmetric bubble that is pretreated with the RAGs, we found an interesting difference. At a P1 concentration of 0.01 U, a substantial amount of the substrate DNA (20%) is protected

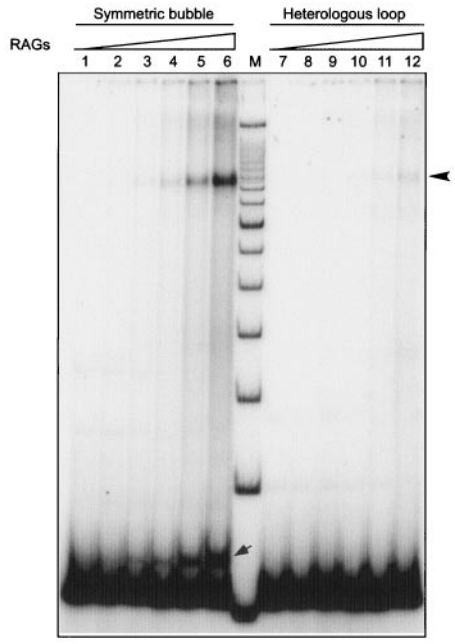

FIG. 8. RAGs bind symmetric bubble and heterologous loop DNA structures. Increasing concentrations of RAG complexes were incubated with [γ-^{32}P]ATP end-labeled 50-bp ds oligomers containing a symmetric bubble structure or a heterologous loop structure for 10 min at 37°C in buffer A in the presence 1 μM 45-bp double-stranded nonspecific DNA. The reaction products were then resolved on a 6% native polyacrylamide gel. In both the symmetric bubble structure and heterologous loop structure panels, the lanes are as follows: lanes 1 and 7, 50-bp DNA containing the non-B DNA structure treated with 0 ng RAGs; lanes 2 and 8, 10 ng RAGs; lanes 3 and 9, 25 ng RAGs; lanes 4 and 10, 50 ng RAGs; lanes 5 and 11, 100 ng RAGs; lanes 6 and 12, 200 ng RAGs; lane M, 50-bp ladder. The band resulting from the RAG binding with the specified structure is indicated by the arrowhead. The new band generated due to the nicked bubble structure is indicated by a small arrow near the bottom of the gel.

from P1 nuclease digestion (Fig. 10A, compare lanes 6 and 7; compare also lane 7 with lane 2). A further increase in the P1 concentration (0.1 U) also was not sufficient to completely digest the bubble structure further, suggesting that the RAGs might be binding to the single-stranded region (Fig. 10A, lane 8). These results reveal that, though 0.01 U of the P1 nuclease is sufficient to digest the bubble structure, when RAGs are prebound that concentration is not sufficient to achieve a similar digestion. This indicates that RAGs might be binding to the single-stranded region at least partially; otherwise, one would not have found any effect on P1 nuclease digestion after the RAG pretreatment. Another interesting part of the study is that, upon preincubation with the RAGs, we found a new band above the 50-bp substrate DNA level (see above) (Fig. 10A, compare lanes 1 and 6). The studies described above suggested that this band is due to RAG nicking on one of the strands of the bubble. Upon incubation with the P1 nuclease, we found a reduction in the molecular weight of this band, probably because of removal of a few nucleotides from the nicked end of the bubble structure (Fig. 10A, compare lanes 6 and 7). These results further indicate that RAGs may be binding at least a part of the single-stranded region of the bubble.

In an independent study, the P1 digestion pattern of the symmetric bubble structure was further analyzed on a denaturing PAGE (15%). Consistent with the above results, we found that upon preincubation with the RAGs, P1 nuclease was not accessible to the single-stranded region of the symmetric bubble structure (Fig. 10B, compare lanes 1 to 5 with lanes 6 to 10). These results and those above indicate that the RAG complex is binding at least a portion of the single-stranded region of the bubble, in addition to the double-stranded DNA. RAG complex binding to the transition between the single- and double-stranded DNA is likely to be the basis for the protection of the single-stranded DNA and for the targeting of RAG nicking to the double-stranded regions nearest to those transitions.

DISCUSSION

In the present study, we have shown that the RAG complex is able to create DSBs in the bcl-2 Mbr, rather than merely the single-strand nicks that we were previously able to document only on the bottom strand (31). The RAG complex cleaves the non-B form DNA at the Mbr, but not the duplex (B-DNA) form. The non-B structure formation is a prerequisite for the RAG cleavage, as there is no RAG-induced DSB formation in the absence of the non-B structure conformation. RAGs are also able to bind and nick other non-B DNA structures, leading to double-strand break formation.

End configuration of the cleavage by RAGs at the bcl-2 Mbr. Our earlier study was limited in two ways: (i) we were unable to explain the lack of RAG nicking on the top strand and (ii) we did not know how a nick on the bottom strand is converted to a DSB (which would be required for the bcl-2 translocation). The present study shows that RAGs are able to create DSBs that can be detected on a native gel. Further, RAG cleavage sites on the top and bottom strands can be observed on a denaturing gel, resulting in DSBs. This argues that the DSBs created at the bcl-2 Mbr are due to two independent nicks and not due to a misrecognition of any heptamer/nonamer-like sequence at the Mbr (see below).

In a previous study, we only documented nicks on the bottom strand of supercoiled and linearized plasmid at the Mbr. At that time, we only examined the top strand using supercoiled DNA, and we did not see any nicks. Based on that, we did not proceed to examine linearized plasmid DNA. The current study used short linear DNA molecules, and here we were able to observe the nicks on both the top and bottom strands. One possible explanation that we favor is that supercoiling disfavors nicking on the top strand at the specific locations where we observe nicking on the short linear DNA fragments. Supercoiled substrate may have structural features that block RAG cleavage at some positions or disperse it over a length that is not possible to detect. Regarding the last point, in order to detect a nick by primer extension, a minimum number of molecules must have the nick at that same position. Dispersal over a broader region can lower the signal to a point that is undetectable.

Non-B DNA structure formation is essential for RAG-induced double-strand breaks at the bcl-2 Mbr. Our results show that when structure formation is abolished at the bcl-2 Mbr by GGG→CCC exchange upstream of peak I, we do not see any RAG-induced DSBs. Similarly, on a control DNA fragment

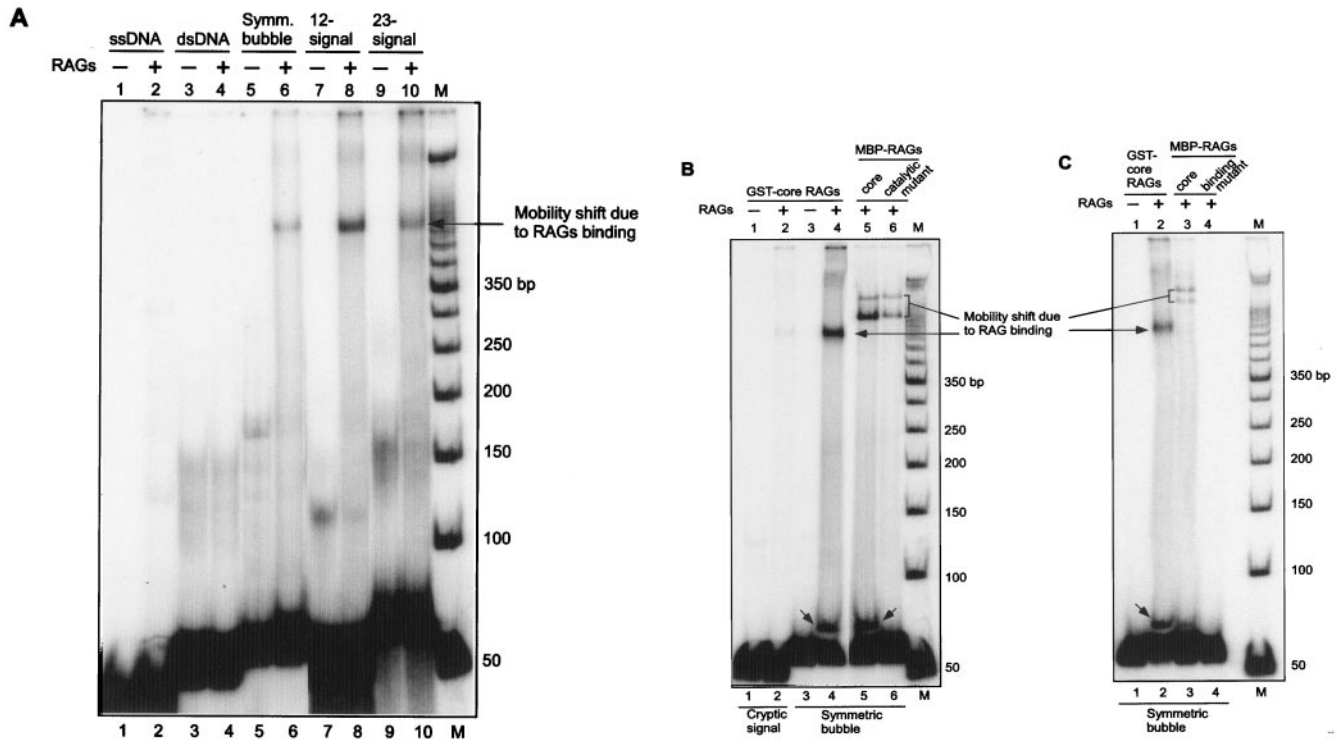

FIG. 9. RAG binding occurs only when a non-B DNA structure or V(D)J recombination signal is present. RAGs (100 ng) were incubated with end-labeled 50-bp ds oligomer for 10 min at 37°C as described above. The reaction products were then resolved on a 6% native polyacrylamide gel. A. Comparison of RAG binding on duplex DNA, symmetric bubble, and 12-/23-signals. Single-stranded DNA was used in lanes 1 and 2. A 50-bp double-stranded DNA was prepared by annealing YM21 and SCR174 (lanes 3 and 4). A symmetric bubble structures (lanes 5 and 6) was prepared as described in Materials and Methods. The 12-signal was prepared by incubating KY28 and KY29, and the 23-signal was prepared by incubating KY36 and KY37. The shifted band is indicated by the arrow. Symm. Bubble, symmetric bubble. Core GST-RAGs were used for the RAG binding studies. Intervening lanes were removed between lanes 6 and 7. B. Comparison of RAG binding in the presence of GST and MBP-RAG preparations. "Cryptic signal" indicates that the sequence of the heptamer and nonamer varies from the standard V(D)J signal sequence (lanes 1 and 2). The core GST-RAGs were used in lanes 1 to 4. Core MBP-RAGs were used for binding studies in lane 5. The core MBP-RAG1 active site mutant and core MBP-RAG2 were used in lane 6. Intervening lanes of no interest were removed between lanes 4 and 5. C. The RAG binding mutant abolishes the binding ability of RAGs on symmetric bubble structures. The MBP-RAGs used are core double-MBP-RAGs (lane 3) and core double-MBP-RAG1 binding mutant/core double-MBP-RAG2 (lane 4). In all three panels, the shifted bands are indicated by arrows. The new band generated due to nicked bubble is indicated by a small arrow near the bottom of the gel.

where there is no structure formation, we do not see double-strand breakage by RAGs. These data indicate that RAG cleavage is directly correlated with the presence or absence of the structure at the Mbr. If the RAG cleavage were due to any kind of heptamer/nonamer-like sequence at the bcl-2 Mbr, one should not see such a dependence on the non-B structure. The difference between the Mbr and the mutant-Mbr fragment is only an alteration of 3 bp, and it is over 50 bp away from the nearest CAC sequence. Hence, the 3-bp change is an effect on DNA structure, as we have shown in two previous studies (18, 21).

Consistent with our earlier studies of RAG cleavage on plasmid DNA, we have shown that the RAG cleavage is totally abolished if we replace the core RAGs with mutant RAGs. This indicates that the cleavage activity observed is due to the RAGs themselves and not due to any copurifying nuclease.

Features of the bcl-2 Mbr structure that are targeted by the RAG complex. It is important to note that we see a reduction in the quantity of shifted species (non-B form DNA) proportional to the increase in RAG concentration. We do not see any significant reduction in the quantity of duplex DNA. Hence, the non-B form DNA structure at the bcl-2 Mbr is the substrate for RAG cleavage.

What feature of the non-B structure is the RAG complex recognizing for its cleavage? Our earlier study using gel shift assays indicated that there are two different major structures at the bcl-2 Mbr at peak I or at peak III, one upstream of peak I (major peak I conformation) and the other downstream of peak I (minor conformation) (28). The analysis of RAG cutting on a denaturing gel shows that RAG cleavage sites, for the most part, match with the location of non-B structure formation. On a 248-bp fragment, the structure formation occurs upstream of peak I. All of the RAG cleavage sites (except one) fall at or near the sequence where the structure exists (Fig. 2). It appears that most of the RAG cleavage sites are at the junction of duplex DNA with the non-B form DNA (or within a few nucleotides of this junction).

Comparable results were obtained at peak I of a 339-bp fragment. However, our previous study determined that this fragment can form two structures, one at peak I and the other at peak III (28). We do not see RAG cleavage activity at peak III. It may be that when RAGs cleave first at the peak I

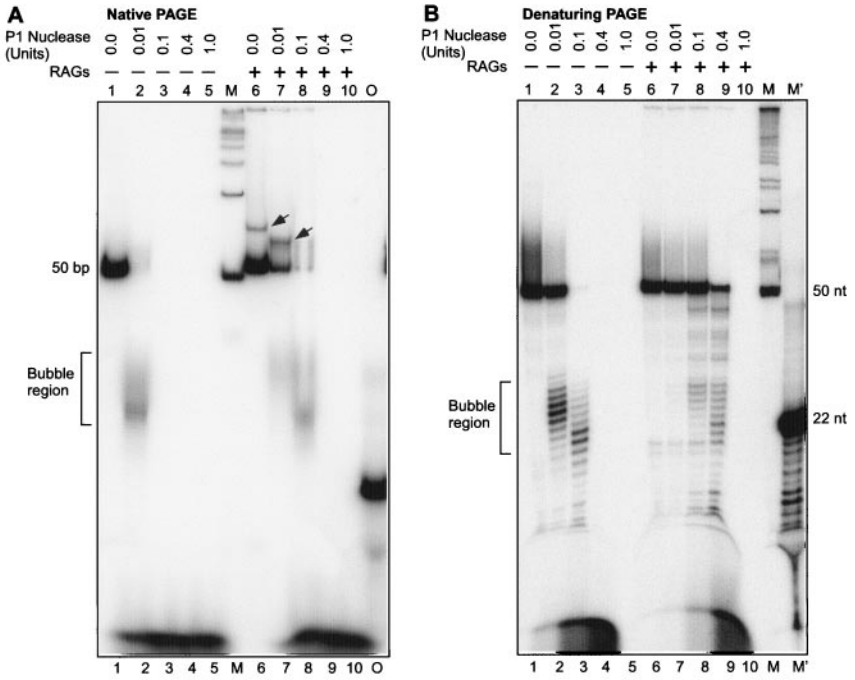

FIG. 10. P1 nuclease assay showing binding of RAGs to the single-stranded region of the symmetric bubble. Increasing concentrations of P1 nuclease were incubated with a [γ-^{32}P]ATP end-labeled 50-bp ds oligomers containing a symmetric bubble structure, with and without pretreatment with RAGs (100 ng of RAGs treated for 10 min at 37°C, in a volume of 15 μl) in buffer A for 15 min for 37°C. The reaction products were then resolved either on a 15% native polyacrylamide gel (A) or a 15% denaturing polyacrylamide gel (B). In both panels, lanes 1 to 5 contain no RAGs and lanes 6 to 10 are with RAGs. The shifted band due to the nicked bubble is indicated by an arrow in panel A. Lane M, 50-bp ladder; lane M′, 22-nt oligomer digested with Klenow to generate a ladder; lane O, [γ-^{32}P]ATP-labeled 22-nt oligomer. The bubble region is indicated by the bracket.

structure, the peak III structure may become destabilized, so that it is no longer a target site for RAG cleavage.

In the in vitro studies, we did find a nick at a CAC site close to peak II of the bcl-2 Mbr on a denaturing gel. Interestingly, this nick is not converted to a double-strand break; otherwise, we would have seen evidence of a DSB on the native gel.

Recently, it has been shown that some translocation breakpoint boundaries are near the site of a predicted cruciform structure in bacteria, and these deletions are dependent on mismatch repair (2). At the bcl-2 Mbr, the non-B structure is not a cruciform and, importantly, is not induced by transcription (28, 31). Moreover, the bcl-2 Mbr break occurs in mitotic cells that become neoplastic, rather than in the meiotic cells that result in constitutional translocations. Finally, the translocation at the bcl-2 Mbr is RAG dependent (31). Hence, the events at the bcl-2 Mbr appear to bear no relation to events at possible cruciforms.

The RAG-induced cleavage observed by us is different from the situation where the RAGs use the 3′-OH of a signal end to attack a 3′ overhang (27). In the present study, we incubated the Mbr or other non-B DNA regions only with the RAG complex, not with any signal ends. This ruled out the possibility that the 3′-OH of a signal end complex is used as a nucleophile in a phosphodiester cleavage.

RAGs bind and induce nicks and double-strand breaks on other non-B DNA structures. The ability of RAGs to nick at or near transitions between double-stranded and single-stranded DNA on both symmetric bubble structures and on heterologous loop structures is interesting. Earlier RAG studies reported that the RAGs are able to nick within a hairpin structure in Mn^{2+} buffer (4) or much more weakly in Mg^{2+} buffer (37). In the present study, we showed that RAGs are capable of inducing nicks at multiple locations within the double-stranded region of different non-B DNA structures. Similarly, the RAG nicking occurs at multiple locations within the Mbr (Fig. 11). Such a property of the RAGs may relate to how they distort DNA near the signal–coding-end transition region for the physiologic nicking event in V(D)J recombination (32). Another interesting aspect of the present study is that the RAG cleavage on non-B DNA structures occurs under physiological (in the presence of Mg^{2+}) buffer conditions. Others have also reported that RAGs are capable of nicking in the double-stranded region near single-strand–double-strand transitions in DNA with 3′ overhangs (11, 35) (Fig. 11).

RAGs recognize non-B structures as a binding target. Though we were not able to find RAG binding on the bcl-2 Mbr DNA structures, we were able to detect the RAG binding on both symmetric bubble and heterologous loop structures. This may be because the Mbr non-B DNA structure exists in only 10 to 15% molecules, while symmetric bubble and heterologous loop structures exist in all molecules (100%). The RAG binding on symmetric bubbles is only twofold lower than the binding of RAG complexes to standard V(D)J heptamer/nonamer signals.

We found that a RAG active site mutant does not have any effect on the RAG binding in the case of symmetric bubble

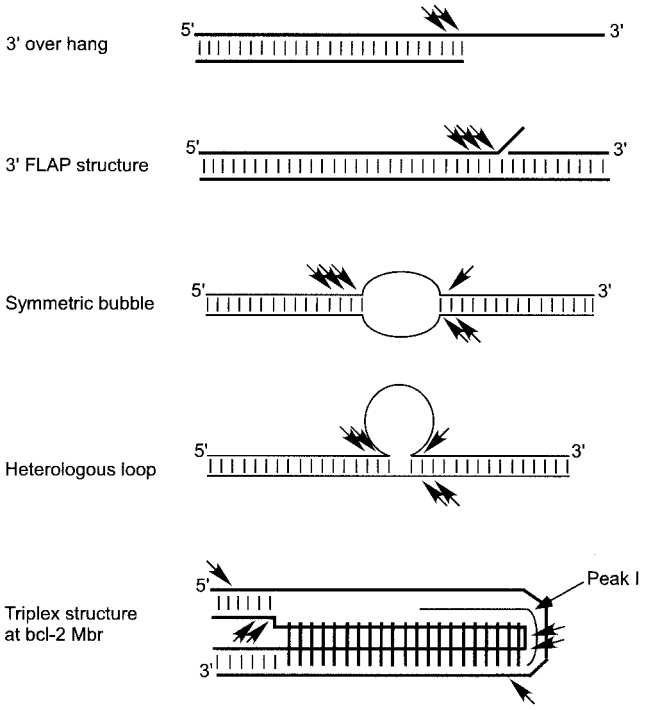

FIG. 11. Comparison of RAG cleavage activity on different 3′ overhang and non-B DNA structures under physiologic buffer conditions. RAGs cleave at one or two positions on 3′ overhang DNA substrates at the duplex–single-stranded junctions (35). RAGs also cleave 3′ FLAPs at multiple locations at the duplex–single-stranded transitions (11, 35). The present study shows that RAGs are able to cleave different non-B DNA structures, such as triplex DNA, symmetric bubbles, and heterologous loop structures. Physiological concentrations of Mg^{2+} were used in all the RAG cleavage experiments. Small vertical bars between horizontal lines represent Watson and Crick hydrogen bonds. Long vertical bars shown in the triplex structure represent Hoogsteen hydrogen bonds. RAG nicking positions are indicated by arrowheads.

structures, just as was the case for V(D)J recombination signal sequences. Correspondingly, the RAG binding mutant, which does not bind to the V(D)J signal sequence, is also unable to bind to the non-B DNA structure. These results indicate that, despite differences in the target substrates, the binding and cleavage domains used by the RAG complex are the same.

Because RAGs are able to cleave other non-B DNA structures like bubble structures, how often would such structures be encountered by RAGs in the genome? The RAG2 protein is only stable during G_0/G_1 of the cell cycle (21, 22); hence, there is no possibility of RAG activity on non-B structures during DNA replication. During G_1, single RAG-generated nicks at cryptic genomic sites may be religated by repair machinery. Only when there are nearby nicks on both strands, as in the case of the bcl-2 Mbr, would such RAG activity lead to DSBs.

RAG binding to non-B structures is likely to require single-stranded regions. It has been proposed that even in the case of signal sequences, DNA unwinding may be occurring at the heptamer region (32). As the single-stranded region occupied by RAGs in the symmetric bubbles appears to be short, the RAGs may be binding partly to single-stranded regions and partly to double-stranded regions.

Is there any mechanistic relationship between standard V(D)J recombination, RAG transposition, and the RAG-mediated cleavage at the bcl-2 Mbr? All of the chemical reactions catalyzed by the RAG complex involve use of a hydroxyl group (either as part of a water molecule or a 3′-OH of a signal end) to carry out a nucleophilic attack on a phosphodiester bond (38). Notwithstanding this common active-site chemistry, the mechanism of double-strand break induction by RAGs at the Mbr is quite different from DSB induction in standard V(D)J recombination and in the RAG transposition reaction. Among the numerous differences are the following. First, the overall outcome of the bcl-2 translocation has no similarity to standard V(D)J recombination (which involves deletion or inversion) or transposition (which involves insertion of signal ends). Second, standard V(D)J recombination begins with a nick 5′ of a CAC sequence within the heptamer; this does not occur at the bcl-2 Mbr. Third, the events at the bcl-2 Mbr involve two nicks that are displaced from one another, whereas both standard V(D)J recombination and the RAG transposition reaction involve the use of a 3′-OH as a nucleophile in a transesterification reaction that inverts the chirality at the target site [the opposite strand in standard V(D)J recombination and a random target site in transposition]. Hence, for these and other reasons, the displaced nicks that lead to a DSB at the bcl-2 Mbr occur in a manner that is quite different from the standard V(D)J recombination or RAG transposition.

Recently, it was suggested that standard nicking of RAGs at heptamer/nonamer signals might have some relationship to RAG-mediated translocations and that they might even be relevant to our observations at the bcl-2 Mbr (16). There are several points that make these suggestions unlikely. Thus far, there are two categories of RAG-mediated translocations. First, the RAG-mediated translocations that involve pairing of two heptamer/nonamer-like signals do not stop at the nicking step. Rather, the RAGs mediate the event just like a standard V(D)J recombination reaction. In the second category, the RAG-mediated staggered nicks that we describe here are located at sequences that are located remote from CAC sequences.

It has also been suggested that RAG-mediated transposition occurs into cruciform sites (17) and that these might bear some relationship to our observations at the bcl-2 Mbr (16). Because the bcl-2 Mbr event does not involve transposition, these observations are not mechanistically related to the events at the bcl-2 Mbr. Moreover, another analysis of cruciform structures suggests that this observation may not be a general one (41).

Is the RAG cleavage in vitro comparable to that which occurs in vivo? The non-B structure formed at the bcl-2 Mbr itself is comparable in vitro and in vivo (31). We previously noted single-stranded regions upstream and downstream of peak I in chromosomal DNA (31). By using a gel shift assay system, we have been able to document the same regions of single-strandedness on small DNA fragments in vitro (28). Similarly, we have seen structure formation at peak III of chromosomal DNA (31) and, more recently, we have been able to reproduce a comparable structure formation at peak III on shorter DNA fragments in vitro (28). In essence, we can reproduce all of the major features of the structure formation

that we observed in chromosomal DNA using in vitro gel shift assays.

There is also overall similarity between the location of the nicks on the top and bottom strands of the bcl-2 Mbr and the propensity of patient translocations, indicating that RAGs are cleaving in vivo and in vitro in a similar manner. Moreover, the regions of breakpoints observed in patient bcl-2 Mbr regions, on exogenous cellular substrates, and in these in vitro cleavage assays are similar. In vitro we observed RAG cleavage only when the non-B DNA structure was present. We know that the non-B DNA structure exists inside the cells and that it is the target for the RAG activity. The DSB that is induced in vitro is a staggered break. From the patient translocation junctional sequences and junctional DNA sequences of the recombinants, we know that the break induced in vivo is also staggered. All these different lines of evidence indicate that the current in vitro analysis corresponds in important ways to in vivo studies in the chromosome and on minichromosomal substrates (13, 31, 42). However, inferences that we have drawn concerning breakage at the chromosomal Mbr are based on the assumption that our extrachromosomal substrates undergo breakage in the same way. Though the RAGs may be responsible for most of the cleavage at the Mbr, we cannot rule out a minor contribution by a variety of other nucleases.

ACKNOWLEDGMENTS

We thank I. Haworth, and C.-L. Hsieh for advice and suggestions. We also thank K. Yu and other members of the Lieber laboratory for discussions.

This work was supported by NIH grants to M.R.L.

REFERENCES

1. **Agrawal, A., Q. M. Eastman, and D. G. Schatz.** 1998. Transposition mediated by RAG1 and RAG2 and its implications for the evolution of the immune system. Nature **394:**744–751.
2. **Bacolla, A., A. Jaworski, J. E. Larson, J. P. Jakupciak, N. Chuzhanova, S. S. Abeysinghe, C. D. O'Connell, D. N. Cooper, and R. D. Wells.** 2004. Breakpoints of gross deletions coincide with non-B DNA conformations. Proc. Natl. Acad. Sci. USA **101:**14162–14167.
3. **Bakhshi, A., J. J. Wright, W. Graninger, M. Seto, J. Owens, J. Cossman, J. P. Jensen, P. Goldman, and S. J. Korsmeyer.** 1987. Mechanism of the t(14;18) chromosomal translocation: structural analysis of both derivative 14 and 18 reciprocal partners. Proc. Natl. Acad. Sci. USA **84:**2396–2400.
4. **Besmer, E., J. Mansilla-Soto, S. Cassard, D. J. Sawchuk, G. Brown, M. Sadofsky, S. M. Lewis, M. C. Nussenzweig, and P. Cortes.** 1998. Hairpin coding end opening is mediated by the recombination activating genes RAG1 and RAG2. Mol. Cell **2:**817–828.
5. **Buchonnet, G., F. Jardin, N. Jean, P. Bertrand, F. Parmentier, S. Tison, S. Leprete, N. Contenin, P. Lenain, A. Stamatoullas-Bastard, H. Tilly, and C. Bastard.** 2002. Distribution of bcl-2 breakpoints in follicular lymphoma and correlation with clinical features: specific subtypes or same disease? Leukemia **16:**1852–1856.
6. **Elkin, S. K., A. G. Matthews, and M. A. Oettinger.** 2003. The C-terminal portion of RAG2 protects against transposition in vitro. EMBO J. **8:**1931–1938.
7. **Felix, C. A.** 2001. Leukemias related to treatment with DNA topoisomerase II inhibitors. Med. Pediatr. Oncol. **36:**525–535.
8. **Friedberg, E. C., G. C. Walker, and W. Siede.** 1995. DNA repair and mutagenesis. ASM Press, Washington, D.C.
9. **Fugmann, S. D., A. I. Lee, P. E. Shockett, I. J. Villey, and D. G. Schatz.** 2000. The RAG proteins and V(D)J recombination: complexes, ends, and transposition. Annu. Rev. Immunol. **18:**495–527.
10. **Gellert, M.** 2002. V(D)J recombination: RAG proteins, repair factors, and regulation. Annu. Rev. Biochem. **71:**101–132.
11. **Grawunder, U., and M. R. Lieber.** 1997. A complex of RAG-1 and RAG-2 persists on the DNA after single-strand cleavae at V(D)J recombination signal sequences. Nucleic Acids Res. **25:**1375–1382.
12. **Hiom, K., M. Melek, and M. Gellert.** 1998. DNA transposition by the RAG1 and RAG2 proteins: a possible source of oncogenic translocations. Cell **94:**463–470.
13. **Jager, U., S. Bocskor, T. Le, G. Mitterbauer, I. Bolz, A. Chott, A. Kneba, C. Mannhalter, and B. Nadel.** 2000. Follicular lymphomas BCL-2/IgH junctions contain templated nucleotide insertions: novel insights into the mechanism of t(14;18) translocation. Blood **95:**3520–3529.
14. **Karanjawala, Z. E., N. Murphy, D. R. Hinton, C.-L. Hsieh, and M. R. Lieber.** 2002. Oxygen metabolism causes chromosome breaks and is associated with the neuronal apoptosis observed in double-strand break repair mutants. Curr. Biol. **12:**397–402.
15. **Kirsch, I. R. (ed.).** 1993. The causes and consequences of chromosomal translocations. CRC, Boca Raton, Fla.
16. **Lee, G. S., M. B. Neiditch, S. S. Salus, and D. B. Roth.** 2004. RAG proteins shepherd double-strand breaks to a specific pathway, suppressing error-prone repair, but RAG nicking initiates homologous recombination. Cell **16:**171–184.
17. **Lee, G. S., M. B. Neiditch, R. R. Sinden, and D. B. Roth.** 2002. Targeted transposition by the V(D)J recombinase. Mol. Cell. Biol. **22:**2068–2077.
18. **Lewis, S. M.** 1994. The mechanism of V(D)J joining: lessons from molecular, immunological and comparative analyses. Adv. Immunol. **56:**27–150.
19. **Lewis, S. M., E. Agard, S. Suh, and L. Czyzyk.** 1997. Cryptic signals and the fidelity of V(D)J joining. Mol. Cell. Biol. **17:**3125–3136.
20. **Lieber, M. R.** 1993. The role of site-directed recombinases in physiologic and pathologic chromosomal rearrangements, p. 239–275. *In* I. Kirsch (ed.), The causes and consequences of chromosomal aberrations. CRC Press, Boca Raton, Fla.
21. **Lin, W.-C., and S. Desiderio.** 1994. Cell cycle regulation of RAG-2 V(D)J recombinase. Proc. Natl. Acad. Sci. USA **91:**2733–2737.
22. **Lin, W.-C., and S. Desiderio.** 1993. Regulation of V(D)J recombination activator protein RAG-2 by phosphorylation. Science **260:**953–959.
23. **Marculescu, R., T. Le, P. Simon, U. Jaeger, and B. Nadel.** 2002. V(D)J-mediated translocations in lymphoid neoplasms: a functional assessment of genomic instability by cryptic sites. J. Exp. Med. **195:**85–98.
24. **Melek, M., and M. Gellert.** 2000. RAG 1/2-mediated resolution of transposition intermediates: two pathways and possible consequences. Cell **101:**625–633.
25. **Messier, T. L., J. P. O'Neill, S.-M. Hou, J. A. Nicklas, and B. A. Finette.** 2003. In vivo transposition mediated by V(D)J recombinase in human T lymphocytes. EMBO J. **22:**1381–1388.
26. **Myung, K., A. Datta, and R. D. Kolodner.** 2001. Suppression of spontaneous chromosomal rearrangements by S phase checkpoint functions in *Saccharomyces cerevisiae*. Cell **104:**397–408.
27. **Nishihara, T., F. Nagawa, H. Nishizumi, M. Kodama, S. Hirose, R. Hayashi, and H. Sakano.** 2004. In vitro processing of the 3′-overhanging DNA in the postcleavage complex involved in V(D)J joining. Mol. Cell. Biol. **24:**3692–3702.
28. **Raghavan, S. C., S. Houston, B. G. Hegde, R. Langen, I. S. Haworth, and M. R. Lieber.** 2004. Stability and strand asymmetry in the non-B DNA structure at the bcl-2 major breakpoint region. J. Biol. Chem. **279:**46213–46225.
29. **Raghavan, S. C., I. R. Kirsch, and M. R. Lieber.** 2001. Analysis of the V(D)J recombination efficiency at lymphoid chromosomal translocation breakpoints. J. Biol. Chem. **276:**29126–29133.
30. **Raghavan, S. C., and M. R. Lieber.** 2004. Chromosomal translocations and non-B DNA structures in the human genome. Cell Cycle **3:**762–768.
31. **Raghavan, S. C., P. C. Swanson, X. Wu, C.-L. Hsieh, and M. R. Lieber.** 2004. A non-B-DNA structure at the Bcl-2 major break point region is cleaved by the RAG complex. Nature **428:**88–93.
32. **Ramsden, D. A., J. F. McBlane, D. C. van Gent, and M. Gellert.** 1996. Distinct DNA sequence and structure requirements for the two steps of V(D)J recombination signal cleavage. EMBO J. **15:**3197–3206.
33. **Roth, D. B.** 2003. Restraining the V(D)J recombinase. Nat. Rev. Immunol. **3:**656–666.
34. **Roth, D. B., and N. L. Craig.** 1998. VDJ recombination: a transposase goes to work. Cell **94:**411–414.
35. **Santagata, S., E. Besmer, A. Villa, F. Bozzi, J. S. Allingham, C. Sobacchi, D. B. Haniford, P. Vezzoni, M. C. Nussenzweig, Z. Q. Pan, and P. Cortes.** 1999. The RAG1/RAG2 complex constitutes a 3′ flap endonuclease: implications for junctional diversity in V(D)J and transpositional recombination. Mol. Cell **4:**935–947.
36. **Shinkura, R., M. Tian, C. Khuong, K. Chua, E. Pinaud, and F. W. Alt.** 2003. The influence of transcriptional orientation on endogenous switch region function. Nat. Immunol. **4:**435–441.
37. **Shockett, P. E., and D. G. Schatz.** 1999. DNA hairpin opening mediated by the RAG1 and RAG2 proteins. Mol. Cell. Biol. **19:**4159–4166.
38. **Swanson, P. C.** 2004. The bounty of RAGs: recombination signal complexes and reaction outcomes. Immunol. Rev. **200:**90–114.
39. **Swanson, P. C.** 2001. The DDE motif in RAG-1 is contributed in trans to a single active site that catalyzes the nicking and transesterification steps of V(D)J recombination. Mol. Cell. Biol. **21:**449–458.
40. **Tsai, C.-L., and D. G. Schatz.** 2003. Regulation of RAG1/RAG2-mediated transposition by GTP and the C-terminal region of RAG2. EMBO J. **22:**1922–1930.

41. **Tsai, C. L., M. Chatterji, and D. G. Schatz.** 2003. DNA mismatches and GC-rich motifs target transposition by the RAG1/RAG2 transposase. Nucleic Acids Res. **31:**6180–6190.
42. **Wyatt, R. T., R. A. Rudders, A. Zelenetz, R. A. Delellis, and T. G. Krontiris.** 1992. BCL2 oncogene translocation is mediated by a χ-like consensus. J. Exp. Med. **175:**1575–1588.
43. **Yu, K., F. Chedin, C.-L. Hsieh, T. E. Wilson, and M. R. Lieber.** 2003. R-loops at immunoglobulin class switch regions in the chromosomes of stimulated B cells. Nat. Immunol. **4:**442–451.
44. **Yu, K., and M. R. Lieber.** 2000. The nicking step of V(D)J recombination is independent of synapsis: implications for the immune repertoire. Mol. Cell. Biol. **20:**7914–7921.